

Operational Strategies for Energy Storage Systems Connected to the Electric Power Distribution Grid with Photovoltaic Distributed Generation

Bruna C. Ferreira Peres^{1*}, Arthur E. S. Ribeiro^{1*}, Wesley Peres^{2*} and Francisco C. R. Coelho^{2*}

¹Department of Electrical Engineering, Federal University of São João del-Rei - UFSJ, São João del-Rei, Brazil.

²Department of Electrical Engineering, Federal Center of Technological Education of Minas Gerais - CEFET-MG, Belo Horizonte, Brazil.

*Corresponding author(s). E-mail(s): teste.teste@teste.br; arthurribeiro.ufsj@gmail.com; wesley.peres@ufsj.edu.br; franciscocoelho@ufsj.edu.br;

Abstract

This paper introduces an operational strategy for managing Battery Energy Storage Systems (BESS) integrated into distribution networks with photovoltaic distributed generation (PV-DG). The primary aim is to reduce the negative impacts caused by high PV penetration, such as voltage rise, phase imbalance, and excessive wear on voltage control devices. To address these challenges, a multi-objective control methodology is proposed. The approach focuses on simultaneously optimizing three key aspects: (i) minimizing voltage violations, (ii) decreasing phase unbalance, and (iii) reducing the number of operations performed by automatic voltage regulators. To solve this complex optimization problem, two metaheuristic algorithms—NSGA-II and MOPSO—are employed. The test system is a three-phase, 34-bus distribution network with embedded PV-DG. Electrical modeling and simulation are performed using the OpenDSS platform, while Python scripts are used to automate the optimization process. The

results show that the proposed control strategy significantly enhances power quality and improves the operational efficiency of the network.

Keywords: energy storage, distributed generation, optimization, OpenDSS, NSGA-II, MOPSO.

1 Introduction

In the past two decades, the urgency to mitigate greenhouse gas emissions and diversify the energy mix has driven both global and national policies in favor of renewable energy sources [1]. In Brazil, the National Electric Energy Agency (ANEEL) consolidated guidelines for micro- and mini-generation [2] and, more recently, enacted the regulatory framework for distributed micro-generation, securing the benefits of the Electric Energy Compensation System until 2045 and lowering network usage tariffs for solar projects, thereby strengthening legal certainty in the sector [3]. Recent studies project that the country's installed photovoltaic distributed generation capacity will exceed 20 GW by 2025, driven by declining module prices, financing incentives, and updated tariff structures [4].

Despite its environmental and economic benefits, the high penetration of PVDG presents significant operational challenges for distribution networks, such as overvoltages, reverse power flow, and increased frequency of tap changes in on-load tap-changing transformers (OLTCs) [5, 6]. Technological reviews identify Battery Energy Storage Systems (BESS) as a versatile solution to mitigate these impacts [7, 8]. However, regulatory, economic, and control-related uncertainties still hinder the full utilization of these assets [9, 10].

In addition to mitigating voltage fluctuations, BESSs can provide ancillary services such as frequency regulation, load shifting, and support during contingency events [11, 12]. When properly sized and allocated, these systems enhance grid resilience and improve overall energy efficiency. Nevertheless, their deployment requires well-defined control strategies capable of handling the variability of both load and distributed generation. In this context, multi-objective optimization approaches have been used to develop solutions that balance power quality, reliability, and cost-effectiveness [13, 14].

Several studies have shown that combining BESS with intermittent generation contributes to the dynamic balancing of electric power systems. These systems can store energy during periods of low cost or demand and release it in a controlled manner to alleviate peak loads, smooth voltage and frequency variations, or compensate for unexpected disturbances [12]. However, since BESSs still involve significant investment, their operation must be optimized to ensure technical and economic feasibility. To this end, control strategies based on day-ahead planning or real-time monitoring have been explored to

determine the optimal state of charge and the most appropriate operating mode—charging, discharging, or idle [15].

More recent approaches propose automatic triggering mechanisms based on power thresholds to control charging or discharging depending on network conditions [16]. This logic allows BESSs to operate adaptively, increasing efficiency and extending system lifespan, even when battery degradation is taken into account. Furthermore, studies targeting voltage rise mitigation during peak photovoltaic generation have shown that controlling the state of charge can be an effective and low-cost strategy to improve network stability [17].

1.1 Contributions

This paper presents a multi-objective optimization strategy for the day-ahead scheduling of a Battery Energy Storage System (BESS) operating in distribution networks with high photovoltaic generation penetration. The formulation simultaneously considers three objectives: (i) minimizing peak load demand to alleviate line and equipment overloading; (ii) minimizing the number of tap operations in on-load tap changers (OLTCs) to extend their service life; and (iii) minimizing voltage limit violations in the primary distribution network, in compliance with PRODIST requirements. Uncertainties in photovoltaic generation and load profiles are implicitly addressed through operational scenarios, and the proposed approach is evaluated using modified IEEE-34 and IEEE-123 test systems.

The results indicate that the proposed strategy effectively reduces load peaks, mitigates voltage violations, and limits OLTC operations. Simulations on IEEE-34 and IEEE-123 networks demonstrate consistent improvements in network operation, with balanced solutions between performance and power quality.

1.2 Paper Organization

This paper is organized as follows: Section ?? discusses energy storage technologies and their applications in power distribution networks. Section 2 addresses the applicability of storage systems in multi-objective formulations, while Section 3 presents aspects related to the operational costs of battery energy storage systems (BESS). Section 4 focuses on the optimal allocation and sizing of storage devices. In Section 5, the modeling of the electrical system is developed, including the mathematical formulation of the optimization problem. The solution methodology is detailed in Section 6, highlighting the NSGA-II and MOPSO algorithms. Section 7 presents the case studies and analysis of the results obtained in the IEEE-34 and IEEE-123 test systems. Finally, Section ?? provides the conclusions of the study and suggestions for future research, while Appendix A gathers complementary data used in the simulations.

2 Applicability of BESS in Multi-Objective Formulations

The use of Battery Energy Storage Systems (BESS) in distribution networks with distributed generation (DG) has been explored in various optimization approaches, especially those with multiple objectives. Unlike traditional methods that assign the storage system to a single function, multi-objective formulations allow BESS to simultaneously provide services such as peak shaving, voltage control, and reduction in tap changer operations, leading to more efficient resource utilization and improved economic return.

Some studies focus on peak load reduction by adjusting the demand profile to smooth the consumption curve. In [18], residential consumers are involved in a dynamic tariff scheme modeled via a multi-objective mixed-integer linear programming (MOMILP) approach, aiming to reduce both electricity bills and system peak demand. In [19], a control system combining peak shaving and frequency regulation using industrial batteries achieved financial gains surpassing those of conventional models. Similarly, [20] compares mono- and multi-objective evolutionary algorithms, applying fuzzy logic control experimentally validated in a real network.

In the context of voltage regulation, [21] propose a strategy to minimize energy costs and maintain voltages within regulatory limits in PV-based networks using distributed BESS. Simulations on an IEEE-37 feeder showed that the distributed approach outperformed centralized control. In [22], the deployment of a real BESS unit (0.6 MW/0.76 MWh) effectively mitigated voltage fluctuations and improved regulation response time.

Regarding the reduction of OLTC switching operations—which are stressed by generation variability—[23] highlight the impact of power flow reversals on equipment longevity. In [24], a two-stage fuzzy optimization method is proposed to balance multiple objectives (peak load, voltage profile, losses, equipment wear, and charge/discharge cycles), validated both on IEEE test systems and a real network with a 2 MWh BESS.

Other studies, such as [25] and [26], emphasize the value of multi-objective formulations in dealing with uncertainties in load and generation. The former proposes a hybrid PV/wind system with batteries and supercapacitors, while the latter applies the AA-NSGAII algorithm to reduce power losses and voltage deviations under seasonal scenarios. Both works reinforce the potential of BESS to enhance technical performance and economic efficiency in distribution networks.

3 Operational Costs

The operational costs associated with Battery Energy Storage Systems (BESS) vary depending on the application, installed capacity, and the chosen technology. Although battery prices have declined in recent years, the initial

investment still poses a significant challenge, particularly for small-scale applications. As noted by [27], residential projects tend to have higher unit costs compared to centralized systems implemented by power sector entities.

Several studies have proposed strategies to mitigate these costs. In [28, 29], the authors introduce a coordinated operation method for BESS under scenarios involving potential grid disconnection, operating in isolated (off-grid) mode. The control is based on hourly dispatch schedules and supplemented by thermal storage systems.

In [30], a multi-objective formulation is developed to minimize the total costs of construction, maintenance, and operation in a hybrid system composed of renewable sources, diesel generators, and both stationary and mobile storage units. The solution employs evolutionary algorithms such as GWO, FFA, SCA, and CSA, implemented in the MATLAB environment.

Another notable example is found in [31], where a simultaneous sizing and siting strategy is proposed for BESS and wind turbines. The optimization considers both active and reactive power losses, as well as the cost per installed capacity. Applied to an IEEE 33-bus system, the results showed improved voltage profiles and reduced losses, validating the technical and economic feasibility of the approach.

4 Siting and Sizing of Energy Storage Systems

Proper siting and sizing of energy storage systems (ESS) are critical to ensure both technical performance and economic viability. As highlighted in [32], poorly located or improperly sized ESS units can worsen voltage profiles and increase energy losses, rather than mitigating them. Therefore, planning must consider both electrical and geographical aspects of the distribution network.

In [33], the authors propose a model that determines the optimal placement and capacity of energy storage systems (ESS), taking into account multiple factors such as power losses, voltage fluctuations, and the scheduling of battery charge/discharge over a 24-hour period. Similarly, [34] propose a multi-objective dynamic programming approach for determining the optimal battery sizing in wind-integrated power systems. The results indicate that optimal storage capacity significantly improves energy utilization and reduces operational costs.

In a related study, [35] introduce a sizing method for ESS in wind farms using predictive control, which accounts for output power limits and state-of-charge constraints. Applied to a real wind farm in Fujian, China, the results show that longer dispatch intervals require greater ESS power capacity to effectively manage fluctuations.

5 Modeling and Mathematical Formulation

This work proposes two approaches for the operation of Battery Energy Storage Systems (BESSs) connected to the distribution network with photovoltaic generation. The first approach, implemented in *MatLab*, applies the NSGA-II

and MOPSO algorithms to generate dispatch strategies based on the state of charge (SoC). The second uses OpenDSS, monitoring the active power at the substation to trigger the BESS through logic triggers.

5.1 Mathematical Problem Formulation

This work proposes a multi-objective optimization formulation focused on the operation of Battery Energy Storage Systems (BESSs) connected to the distribution network. The approach aims to minimize three objectives: (i) the peak power supplied by the substation, (ii) the voltage deviation in relation to regulatory limits, and (iii) the number of tap operations of voltage regulators (RTs). The equations associated with the objectives are described in (1)–(4).

$$\min f_1 = \max \left(\sum_{\phi=1}^3 P_{SE}^{\phi,t} \right), \quad \forall t \in T \quad (1)$$

$$\min f_2 = \max(\Delta V_j^{\phi,t}) \quad \forall \phi \in Ph; \forall t \in T; \forall j \in \{\Omega \cup J_B\} \quad (2)$$

with:

$$\Delta V_j^{\phi,t} = \begin{cases} V_j^{\phi,t} - V_{\max}, & \text{if } V_j^{\phi,t} > V_{\max} \\ V_{\min} - V_j^{\phi,t}, & \text{if } V_j^{\phi,t} < V_{\min} \\ 0, & \text{otherwise} \end{cases} \quad (3)$$

$$\min f_3 = N_{TCO} \quad (4)$$

The formulated optimization problem is constrained, and the following non-linear equality and inequality equations represent the physical and operational limitations considered.

$$P_{PV,j}^{\phi,t} - P_{D,j}^{\phi,t} - \sum_{k \in \Omega_j} P_{jk}^{\phi,t} = \left(\frac{SoC_t - SoC_{t-1}}{3\tau} \right) E_B, \quad \forall \phi \in Ph; \forall t \in T; j = J_B \quad (5)$$

$$P_{PV,j}^{\phi,t} - P_{D,j}^{\phi,t} - \sum_{k \in \Omega_j} P_{jk}^{\phi,t} = 0, \quad \forall \phi \in Ph; \forall t \in T; \forall j \in \Omega \quad (6)$$

$$-Q_{D,j}^{\phi,t} - \sum_{k \in \Omega_j} Q_{jk}^{\phi,t} = 0, \quad \forall \phi \in Ph; \forall t \in T; \forall j \in \{\Omega \cup J_B\} \quad (7)$$

$$SoC_{\min} \leq SoC_t \leq SoC_{\max} \quad \forall t \in T \quad (8)$$

$$E_B \cdot (SoC_{-t} - SoC_{-t-1}) \leq P_{\max} \cdot \tau, \quad \forall t_f \in T \quad (9)$$

$$P_{SE}^{\phi,t} \geq 0, \quad \forall \phi \in Ph; \forall t \in T \quad (10)$$

$$SoC_{t_f} = SoC_{t_f-1} + P_{\max} \cdot \tau \quad \forall t_f \in T \quad (11)$$

Where:

- Ph is the set of distribution network phases ($Ph = \{1, 2, 3\}$);
- T is the set of time intervals considered in the simulation ($T = \{1, 2, \dots, t_f\}$);
- Ω is the set of all buses in the system except J_B ;
- J_B is the only bus to which the battery is connected;
- Ω_j is the set of buses connected to bus j ;
- $P_{PV,j}^{\phi,t}$ is the active power injected by the photovoltaic system at bus j , phase ϕ , at interval t (kW);
- $P_{D,j}^{\phi,t}$ is the active power demanded at bus j , phase ϕ , at interval t (kW);
- $P_{jk}^{\phi,t}$ is the active power flow from bus j to bus k , phase ϕ , at interval t (kW);
- $P_{SE}^{\phi,t}$ is the active power supplied by the distribution substation at phase ϕ and interval t (kW);
- E_B is the maximum storage capacity of the battery bank (kWh);
- SoC_t is the state of charge of the battery bank at the end of interval t (%);
- τ is the duration of each time interval considered in the simulation;
- $Q_{D,j}^{\phi,t}$ is the reactive power demanded at bus j , phase ϕ , at interval t (kvar);
- $Q_{jk}^{\phi,t}$ is the reactive power flow from bus j to bus k , phase ϕ , at interval t (kvar);
- SoC_{min} and SoC_{max} are the minimum and maximum state of charge of the battery bank (%);
- P_{\max} is the maximum charge and discharge power of the battery (kW);
- Tap_t^r is the tap position of voltage regulator r at interval t ;
- RT is the set of voltage regulators;
- SoC_{t_f} is the state of charge of the battery bank at the final instant;

Equations (5), (6), and (7) represent the active and reactive power balance at bus j , considering photovoltaic generation and battery operation. The violation of any of these renders the solution infeasible and it is discarded.

Constraint (10) prevents reverse active power flow to the substation, which is considered undesirable. The variable $P_{SE}^{\phi,t}$ corresponds to the power at the substation bus and is handled via penalty in the optimization.

Equation (8) defines the SoC limits of the battery. Constraint (9) limits the variation in SoC according to charge and discharge limits, and equation (11) requires a high final SoC. Since the planning is periodic, these three constraints ensure good BESS performance in subsequent cycles.

5.2 NSGA-II

Bio-inspired heuristics are computational techniques based on patterns observed in nature, developed to solve complex problems [36]. Among them, NSGA-II (Non-Dominated Sorting Genetic Algorithm II) [37] stands out as an advanced version of the traditional genetic algorithm. It adopts a population-based approach to iteratively refine a set of solutions.

The effectiveness of NSGA-II is associated with its evaluation strategy based on the concept of dominance. A solution is considered superior if it improves all objectives or performs better in at least one of them without worsening the others. Additionally, NSGA-II promotes diversity among the solutions, ensuring robustness and representativeness in the final set.

In this study, which involves the optimization of two distinct objectives, the final solutions are visualized on a Pareto curve in a Cartesian plane, as illustrated in Figure 1. Each non-dominated point on this curve represents a unique and optimal solution for a minimization problem.

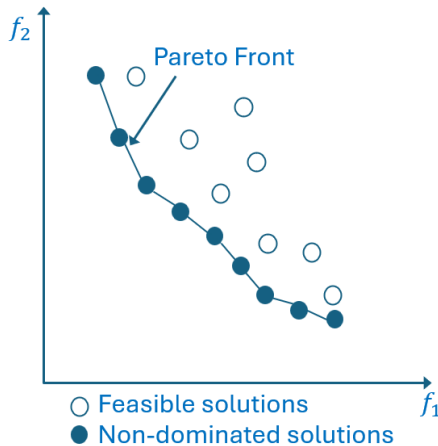


Fig. 1 Illustration of the Pareto Front.

5.3 MOPSO

The Particle Swarm Optimization (PSO) algorithm was initially proposed to solve single-objective optimization problems [38]. Later, it was adapted to handle multiple objectives, resulting in the Multi-Objective Particle Swarm Optimization (MOPSO) algorithm. This work adopts the structure presented in [39], which enhances the diversity in the search for the Pareto front. This adaptation enables simultaneous optimization of multiple objectives, unlike traditional PSO which focuses on only one.

In PSO, each particle in the population seeks to optimize an objective function, adjusting its position and velocity based on two references: its

best historical position and the best global position found by the swarm. In MOPSO, instead of seeking a single optimal solution, particles aim to identify a set of non-dominated solutions forming the Pareto front. This set is stored in a repository that is continuously updated and ranked throughout the iterations.

5.4 Performance Metrics

Performance metrics play a crucial role in evaluating the effectiveness of optimization algorithms, allowing quantitative comparisons between different approaches applied to the same problem. In this research, two metrics were used: cardinality and hypervolume.

Cardinality (σ^2) refers to the number of non-dominated solutions present in the final set. A high value indicates that the algorithm has explored a diverse range of solutions. Conversely, a low cardinality may indicate premature convergence or lack of diversity in the generated solutions.

Hypervolume (σ^3) is a quality metric that evaluates how much the solutions cover the search space. A larger hypervolume indicates a more diverse and higher quality set of solutions, which is especially relevant in multi-objective contexts, where good performance across multiple criteria is sought [40].

5.5 OpenDSS and Storage Model

OpenDSS (Open Distribution System Simulator), developed by EPRI, is an open-source software widely used for simulations in electric distribution systems [41]. It enables both steady-state and dynamic analyses (such as daily power flows) and is compatible with external scripts via the COM interface. Due to its accuracy and versatility, it was recommended by ANEEL for regulatory studies in Brazilian distribution networks.

The storage model implemented in OpenDSS is represented by the *Storage* element, which injects or absorbs active power according to the state of charge (SoC) and the operating mode adopted. The battery power at time t is calculated based on the difference between the current and next SoC, considering the efficiency η , as shown below:

$$P_{BAT}(t) = \begin{cases} (SoC_t - SoC_{t+1}) \cdot \eta, & \text{if discharging} \\ \frac{(SoC_{t+1} - SoC_t)}{\eta}, & \text{if charging} \end{cases} \quad (12)$$

In *Follow* mode, the BESS follows a predefined charge/discharge curve (*LoadShape*), normalized by the battery's nominal power, as shown in equation 13:

$$LoadShape = \left[\frac{P_{BAT}(1)}{P_{Nominal}}, \dots, \frac{P_{BAT}(t_f)}{P_{Nominal}} \right] \quad (13)$$

In *Peak shave* mode, storage operation is controlled by a *StorageController* element that monitors power at a specific network point (P_{monit}) and compares it with the thresholds P_{min} and P_{max} . The control logic is defined as follows:

$$P_{BAT}(t) = \begin{cases} P_{min} - P_{monit}(t), & \text{if } P_{monit}(t) < P_{min} \quad (\text{Charging}) \\ 0, & \text{if } P_{min} \leq P_{monit}(t) \leq P_{max} \quad (\text{Idle}) \\ P_{monit}(t) - P_{max}, & \text{if } P_{monit}(t) > P_{max} \quad (\text{Discharging}) \end{cases} \quad (14)$$

This model allows for the evaluation of different BESS operating strategies in distribution networks with high photovoltaic penetration, enabling better control over demand peaks and voltage variations.

6 Solution via Metaheuristic Optimization and OpenDSS

The solution to the proposed optimization problem combines the use of the NSGA-II and MOPSO algorithms implemented in MATLAB with the electrical simulation performed in OPENDSS. Communication between the platforms is carried out via the COM interface, as shown in Figure 2, allowing each solution proposed by the evolutionary algorithm to be evaluated based on the power flow results.

Each individual p generated by the algorithm represents a sequence of state of charge (SoC) values over the planning horizon, as shown in equation 15:

$$p = [SoC_0, SoC_1, \dots, SoC_{t_f}] \quad (15)$$

In Block 1, the SoC vector p is generated by NSGA-II or MOPSO. In Block 2, it is verified whether each value of SoC_t respects the operational limits defined by equation 8. Block 3 ensures that the variation between two consecutive states respects the maximum charge and discharge power, according to equation 9. Block 4 adjusts the final SoC to a high value, as specified in 11.

In Block 5, vector p is converted into a *LoadShape* vector and sent to OpenDSS. In Block 6, the unbalanced sequential three-phase power flow is performed. Block 7 checks whether the power flow calculation has converged. Otherwise, the individual is penalized in Block 8 by assigning the objective functions f_1, f_2, f_3 the value 10^{100} , as per the criterion in equation 16.

If the flow converges, in Block 9 the objective functions are calculated: f_1 represents the substation demand peak equation 1; f_2 measures voltage deviations equation 2; f_3 counts the number of tap operations of the voltage regulators equation 4.

Blocks 10 and 11 check for the occurrence of reverse power flow at the substation, which triggers the penalization of the objective functions according to equation 16:

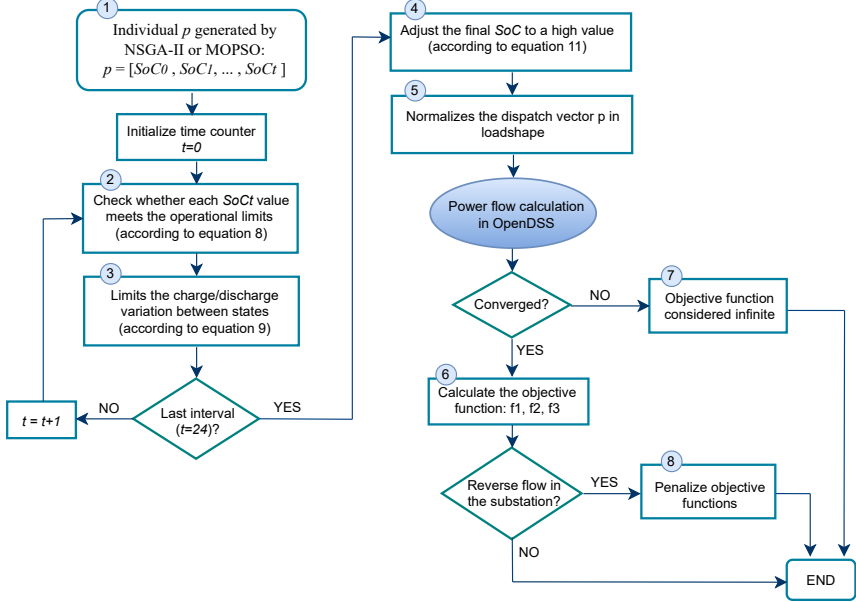


Fig. 2 Solution evaluation flowchart via MatLab and OpenDSS integration.

$$\begin{aligned}
 \min f'_1 &= \max \left(\sum_{\phi=1}^3 P_{SE}^{\phi,t} \right) + 10^6 \cdot \sum_{\phi=1}^3 \sum_{t=0}^{t_f} P_{SE}^{\phi,t}, & \text{if } P_{SE}^{\phi,t} < 0 \\
 \min f'_2 &= \max(\Delta V_j^{\phi,t}) + 10^6 \cdot \sum_{\phi=1}^3 \sum_{t=0}^{t_f} P_{SE}^{\phi,t}, & \text{if } P_{SE}^{\phi,t} < 0 \\
 \min f'_3 &= N_{TCO} + 10^6 \cdot \sum_{\phi=1}^3 \sum_{t=0}^{t_f} P_{SE}^{\phi,t}, & \text{if } P_{SE}^{\phi,t} < 0
 \end{aligned} \quad (16)$$

This process is repeated throughout the generations until the Pareto front is formed with the efficient solutions.

7 Results

This section first describes the tuning parameters of the metaheuristic algorithms, as well as the load and generation profiles selected for the time-series application. Then, the results for the day-ahead dispatch planning of battery energy storage systems (BESS) are presented and analyzed through a comparison of the proposed methods. Both approaches are implemented in IEEE test feeders with 34 and 123 buses using multi-objective algorithms. Finally, active power losses and the influence of the initial state of charge of the battery are evaluated.

The simulations were conducted in MATLAB coupled with OPENDSS v9.4.0.3 through the COM interface for daily power flow calculations. The hardware used was an Intel® Core™ i7-10510U 1.8 GHz, 8GB RAM, Windows10-64bits.

The parameters for each metaheuristic, taken from the literature [20, 42], are listed in Table 1. Population size and number of iterations were kept fixed for both methods; each algorithm was executed 10 times with the same initial population to ensure fair comparison.

Table 1 Metaheuristic algorithm parameters. Source: Author.

Algorithm	Parameter	Value
NSGA-II	Number of iterations	500
	Population size	200
	Crossover probability	90%
	Mutation probability	5%
	Mutation rate	4%
MOPSO	Number of iterations	500
	Population size	200
	Repository size	200
	Inertia weight	0.4
	Global learning coefficient	2
	Personal learning coefficient	2

7.0.1 Load and Generation Profiles

The original IEEE networks (snapshot) were converted to time-series analysis. Residential and industrial loads follow the normalized daily curve shown in Figure 3, typical of *Loadshape*, based on [43]. Each ordinate is multiplied by the nominal power of the corresponding load.

For PV-based distributed generation (PVDG), the *PVSystem* element of *OpenDSS* was used, driven by irradiation and temperature profiles (Appendix A). Generators totaling 45% of the static active demand were installed.

The BESS was modeled using the *Storage* element (95% efficiency, $20\% \leq SOC_t \leq 90\%$) as recommended by [44, 45].

7.1 IEEE-34 Bus System

7.1.1 System Description

The IEEE 34-bus test feeder, illustrated in Figure 4, is a radial system located in Arizona, characterized by large unbalanced load blocks and relatively long distribution lines. Due to significant voltage drops, the feeder is equipped with two automatic voltage regulators and shunt capacitor banks. The network operates mainly at 24.9 kV, with a small 4.16 kV branch powered by a step-down transformer.

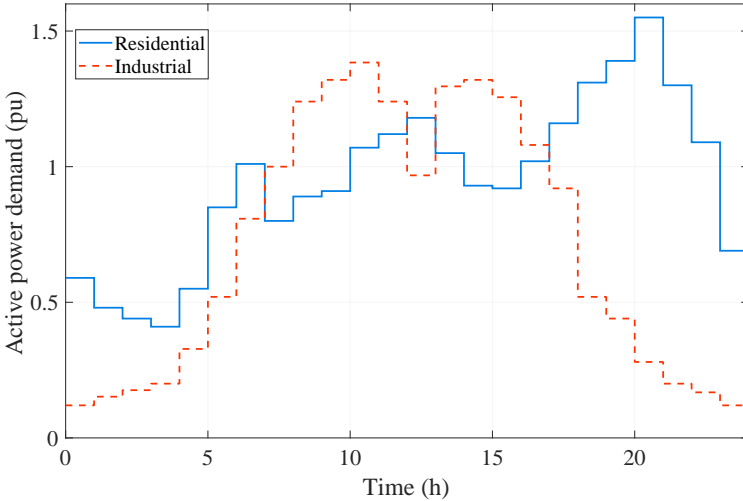


Fig. 3 Typical residential and industrial load curves. Adapted from [43].

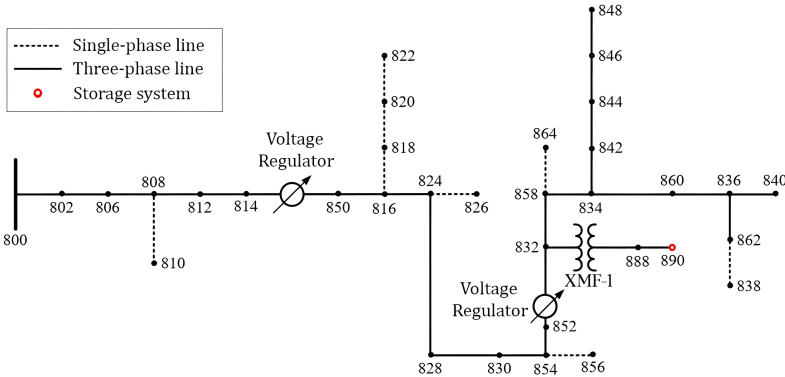


Fig. 4 Single-line diagram of the IEEE 34-bus feeder. Source: Adapted from [46].

Loads at buses 844 and 890 are considered industrial; all others follow a residential profile. The system has an active power demand of 2042 kW and reactive power of 290 kvar. A total of 873 kW of photovoltaic generation was added in single- and three-phase arrays (detailed in Appendix A). The distributed generation is modeled as constant active power injection. A three-phase battery of 2 MWh and 500 kW was installed at bus 890, without reactive power support, according to recommendations from [14, 24].

The automatic voltage regulators have 33 tap positions and start at the central tap. Further system details can be found in [47].

7.1.2 Multi-Objective Optimization Results

Figures 5 and 6 present the Pareto front obtained with the NSGA-II and MOPSO algorithms, considering $SoC_0 = 50\%$. The axes correspond to substation peak power, maximum voltage deviation, and total number of regulator tap changes.

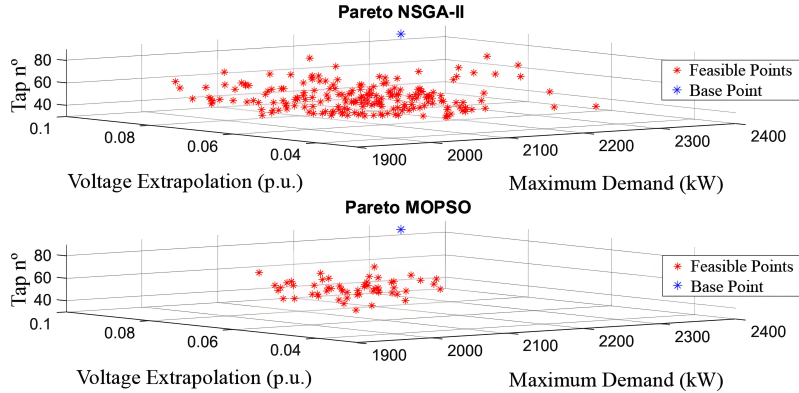


Fig. 5 Pareto-optimal front with $SoC_0 = 50\%$. Source: Author.

Figure 6 presents the same Pareto front from different perspectives. The solution quality is assessed using hypervolume (H) and cardinality (C_R), whose mean and standard deviation are listed in Table 2.

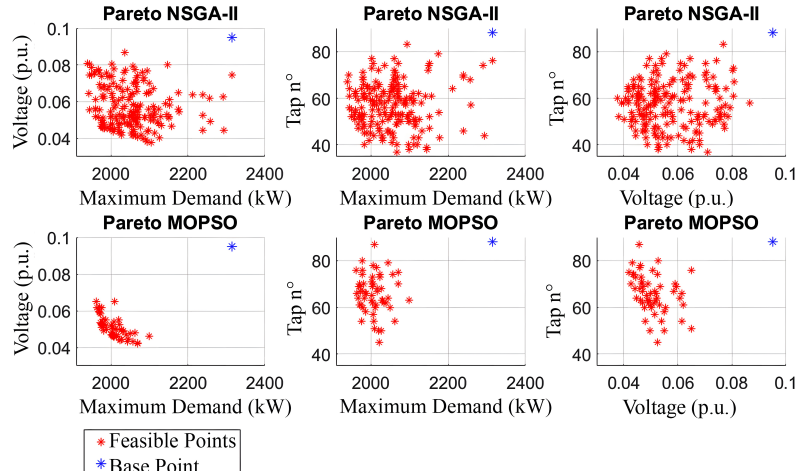


Fig. 6 Pareto front with multiple projections. Source: Author.

Table 2 Quality metrics for 10 executions. Source: Author.

Metric	Algorithm	Mean	Std. Deviation
Hypervolume (H)	NSGA-II	902.8	54.6
	MOPSO	698.1	18.2
Cardinality (C_R)	NSGA-II	199.3	1.1
	MOPSO	54.0	3.4

7.1.3 Comparison with Trigger-Based Strategy

Table 3 provides a direct comparison of selected solutions from NSGA-II, MOPSO, the base case (without storage), and the trigger-based control method. The results highlight the values of the three objective functions: substation peak active power, voltage deviation, and number of regulator tap changes.

Table 3 Selected points for analysis in the IEEE 34-bus system. Source: Author.

Algorithm	F_{obj_1} : Power (kW)	F_{obj_2} : Voltage (pu)	F_{obj_3} : TAP
Base	2314.29	0.095	88
NSGA-II	1966.17	0.053	51
MOPSO	1960.55	0.064	68
Trigger	2019.87	0.084	77

NSGA-II shows the best overall performance, especially in reducing tap operations and voltage deviation. The trigger-based method has the worst results across all metrics. This control relies on two power thresholds: discharge occurs above 1950 kW, charge below 1850 kW, and idle mode in between. The controller aims to maintain substation power near the average of 1900 kW.

Figure 7 displays the substation power import throughout the day. All methods reduce the load peak, particularly between 8 a.m. and 9 a.m. However, for prolonged peaks (10 a.m. to 11 a.m.), the trigger method performs worse, while NSGA-II and MOPSO sustain better control.

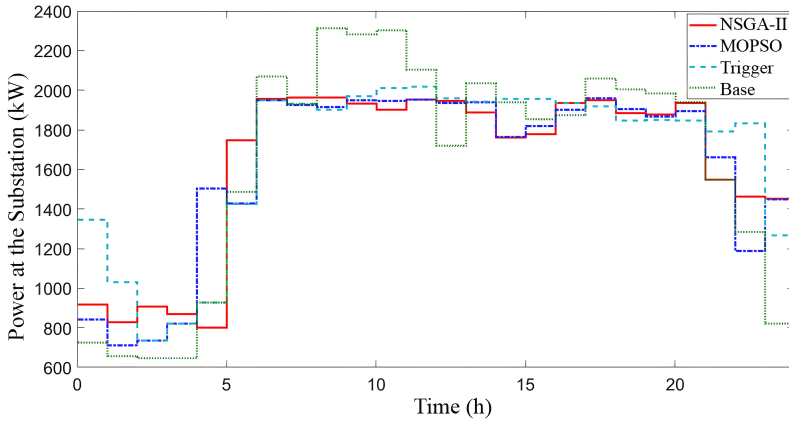
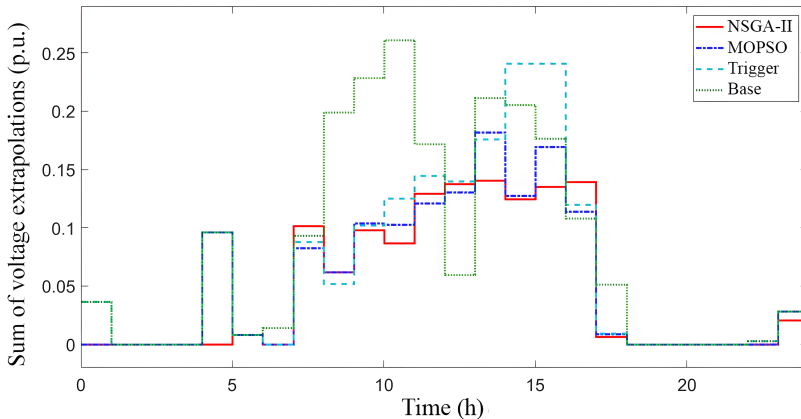
Figure 8 presents the sum of voltage deviations across all buses and phases. NSGA-II is the most effective, followed by MOPSO. The trigger method underperforms, especially from 2 p.m. to 4 p.m.

Figure 9 shows voltage at bus 890 (phase A), where the battery is installed. NSGA-II best mitigates voltage sags between 8 a.m. and 11 a.m. MOPSO violates limits from 4 a.m. to 5 a.m. The trigger method performs worse between 1 p.m. and 4 p.m.

Figure 10 displays voltages at two buses: 814 (near the substation) and 840 (remote). Both remain within regulatory limits, ensuring network stability.

Figure 11 indicates that NSGA-II significantly reduces tap switching, extending equipment life. All strategies outperform the base case.

Figure 12 shows daily battery *SoC* profiles. NSGA-II maintains a higher, more stable charge, benefiting battery lifespan. MOPSO behaves similarly, while the trigger control causes larger fluctuations.

Fig. 7 Substation imported power (kW). Source: Author.**Fig. 8** Sum of voltage deviations across all buses and phases. Source: Author.

7.1.4 Additional Analyses

As previously discussed, the initial state of charge (SoC_0) can affect the performance of the optimization methods, as power limits restrict the variation between consecutive states. Therefore, this section investigates the impact of different initial SoC conditions (25%, 50%, and 75%) on the planning results.

Table 4 presents the average and standard deviation of the hypervolume (H) and cardinality (C_R) metrics obtained from 10 runs for each scenario. It is observed that the initial SoC value has a limited influence on solution quality. This is partly due to the simulation starting during the nighttime, when demand is low, allowing the battery to reach an appropriate charge level before the first peak. This behavior is advantageous for the system operator, as different initial conditions still lead to consistent operational gains.

Fig. 9 Voltage at phase A of bus 890. Source: Author.

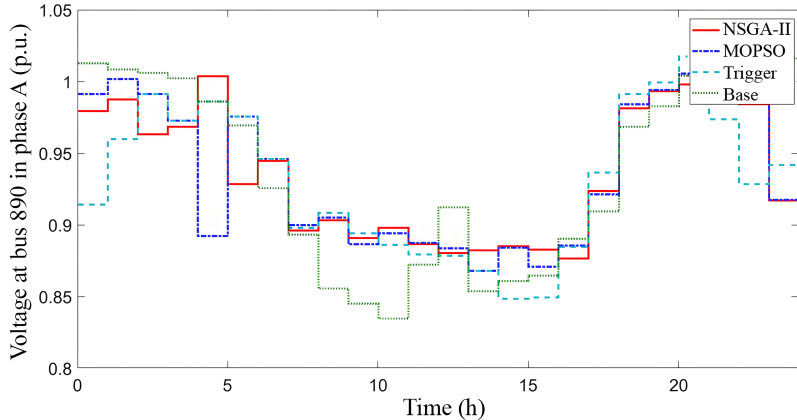
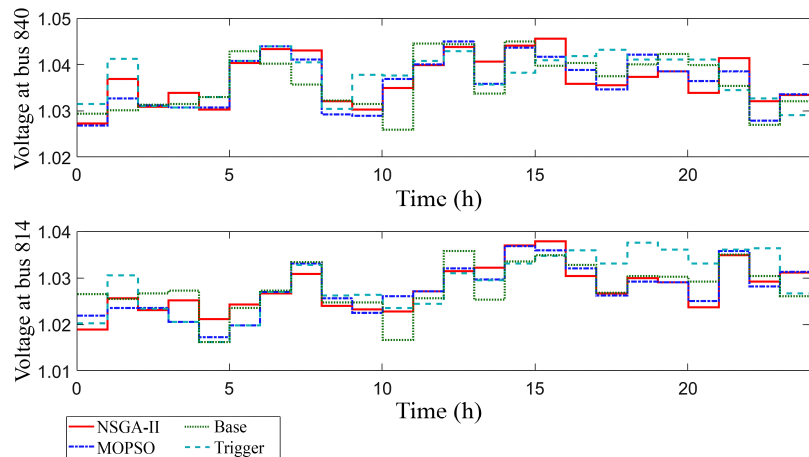


Fig. 10 Voltage at phase A of buses 840 and 814. Source: Author.



In addition, the impact of management strategies on active power losses is evaluated. Table 5 presents the average and standard deviation of daily energy losses for the solutions obtained by NSGA-II and MOPSO, as well as the base case and the trigger-based method.

Although loss minimization was not explicitly included as an optimization objective, both metaheuristics achieved significant reductions compared to the base case. The low standard deviation underscores the robustness of the methods, indicating a consistent trend of energy savings regardless of the selected Pareto solution. These results highlight the potential of storage systems managed by evolutionary optimization to enhance the overall energy performance of distribution networks.

Fig. 11 Tap switching per regulator in the IEEE 34-bus system. Source: Author.

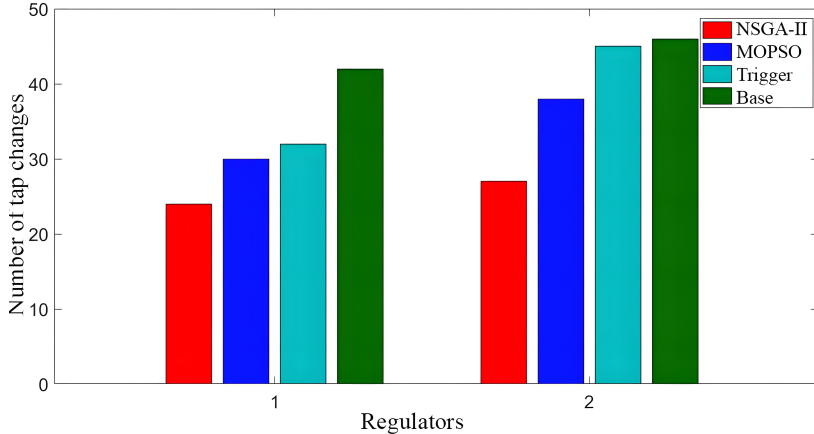
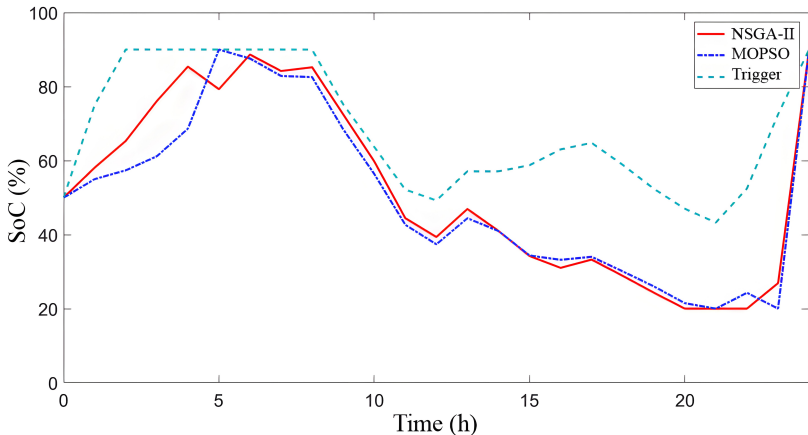


Fig. 12 Battery state of charge (*SoC*) in the IEEE 34-bus system. Source: Author.



7.2 IEEE-123 Bus System

7.2.1 System Description

The IEEE 123-bus system, illustrated in Figure 13, consists of unbalanced loads of different types (constant power, current, or impedance), overhead and underground lines, four voltage regulators, *shunt* capacitors, and switches for network reconfiguration. The network operates at 4.16 kV, except for one bus operating at 0.48 kV. The voltage magnitude must remain between 0.93 pu and 1.05 pu, according to ANEEL [9].

Buses 47, 48, 65, and 76 have industrial loads [43], while the others are residential. Table 6 shows three additional inductive loads used to simulate degraded operating conditions, as proposed in [43].

Table 4 Average and standard deviation of metrics for 10 runs with different initial SoC values in the IEEE 34-bus system. Source: Author.

Metric	Algorithm	SoC_0	Mean	Std. Deviation
Hypervolume (H)	NSGA-II	25%	926.1	14.1
		50%	902.8	54.6
		75%	889.5	13.0
	MOPSO	25%	663.5	25.7
		50%	698.1	18.2
		75%	630.8	15.5
	NSGA-II	25%	199.0	1.7
		50%	199.3	1.1
		75%	199.0	1.7
Cardinality (C_R)	MOPSO	25%	54.3	5.5
		50%	54.0	3.4
		75%	46.3	10.9

Table 5 Active energy losses in the IEEE 34-bus system (in kWh). Source: Author.

	Base	Trigger	MOPSO		NSGA-II	
			Mean	Std. Dev.	Mean	Std. Dev.
Losses (kWh)	5536.06	5483.21	5154.82	61.83	5131.93	58.32

Table 6 Additional loads in the IEEE 123-bus system. Source: [43]

Bus	Phase	Active Power (kW)	Reactive Power (kvar)	Type
46	A	50	20	Residential
97	A	200	80	Industrial
106	A	50	20	Residential

In steady-state mode, the modified system has 3.9 MW of active load and 2 Mvar of reactive load. A total of 1.8 MW of single-phase and three-phase photovoltaic generation was installed in random locations (see Appendix A). A three-phase battery bank with 4 MWh capacity and 1000 kW nominal power was installed at bus 60, located near one of the voltage regulators [48].

7.2.2 Multi-Objective Optimization Results

Figures 14 and 15 show the Pareto front generated by the NSGA-II and MOPSO algorithms with $SoC_0 = 50\%$, including the base solution (blue point). The axes represent peak power, voltage deviation of the most critical bus, and the number of tap changes on voltage regulators.

Table 7 presents the quality metrics. NSGA-II achieved a higher cardinality, while the average hypervolume was similar to that of MOPSO, indicating better distribution.

7.2.3 Comparison with Trigger-Based Logic

For comparison purposes, intermediate solutions obtained by NSGA-II and MOPSO were selected to equalize peak power levels and allow a fair assessment

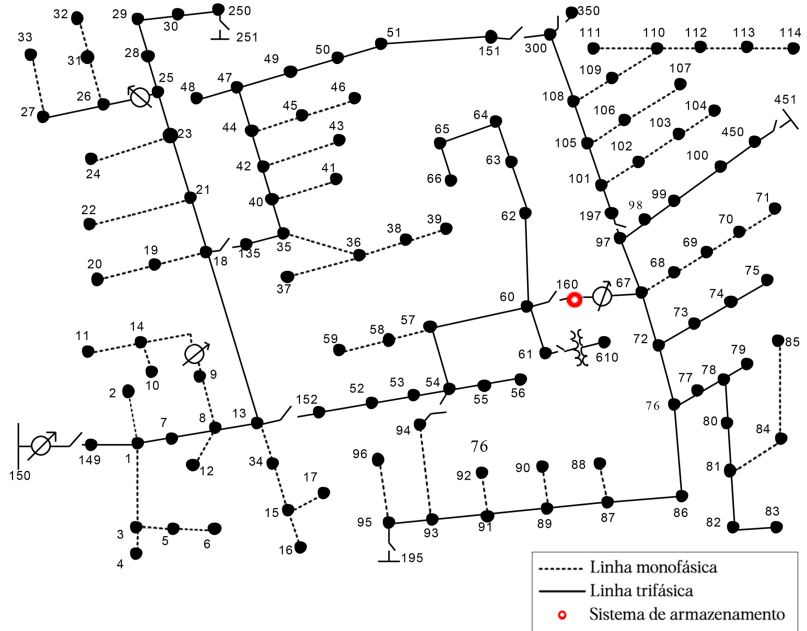


Fig. 13 Single-line diagram of the IEEE 123-bus system. Source: Adapted from [46].

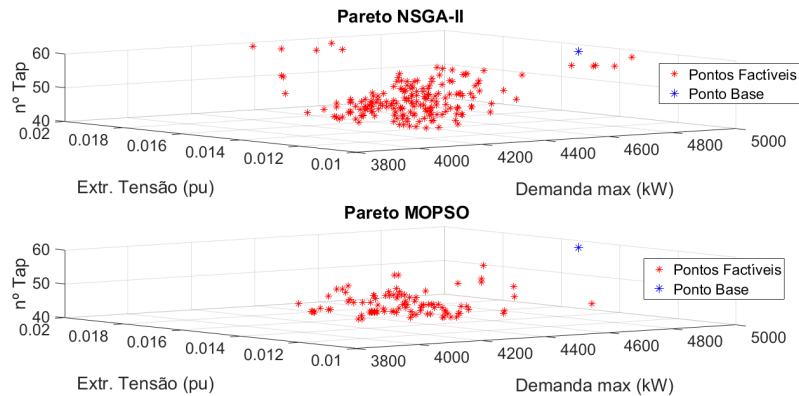


Fig. 14 Pareto front with $SoC_0 = 50\%$. Source: Author.

Table 7 Evaluation metrics for 10 runs with $SoC_0 = 50\%$. Source: Author.

Metric	Algorithm	Average	Std. Dev.
H	NSGA-II	40.81	4.3
	MOPSO	40.54	3.8
C_R	NSGA-II	199.3	1.1
	MOPSO	103.1	6.4

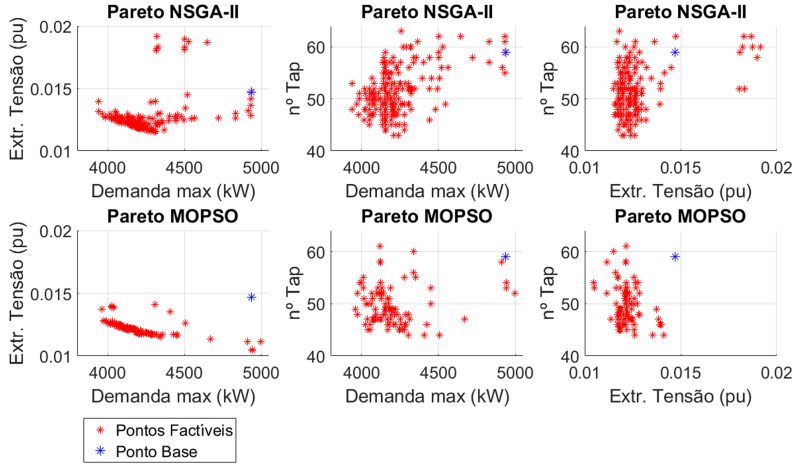


Fig. 15 Projections of the Pareto front with $SoC_0 = 50\%$. Source: Author.

of the methods. Table 8 presents the objective function values for the three analyzed methods (NSGA-II, MOPSO, and Trigger), as well as the base case without storage. NSGA-II stood out for achieving the lowest number of tap changes.

Table 8 Objective functions of the methods. Source: Author.

Algorithm	F_1 (kW)	F_2 (pu)	F_3 (taps)
Base	4934.35	0.014	59
NSGA-II	3973.00	0.012	48
MOPSO	3973.00	0.012	52
Trigger	4073.05	0.013	61

Based on the heuristic solutions, the trigger logic was configured with thresholds of 3500 kW and 3650 kW for charging and discharging modes, respectively. Within this band, the system remains idle. The goal is to maintain substation power close to 3575 kW while respecting battery limits.

Figure 16 illustrates the active power profile imported from the substation throughout the day. Between 5 PM and 10 PM, there is a peak in demand. All methods reduce this peak until approximately 8 PM, after which the performance of the trigger logic declines. This demonstrates its limitation in handling long-duration peaks.

Figure 17 shows the sum of voltage deviations for each time interval, considering all buses and phases. The heuristic methods significantly reduce these deviations, especially between 10 AM and 2 PM, where the trigger logic performs worse than the base case.

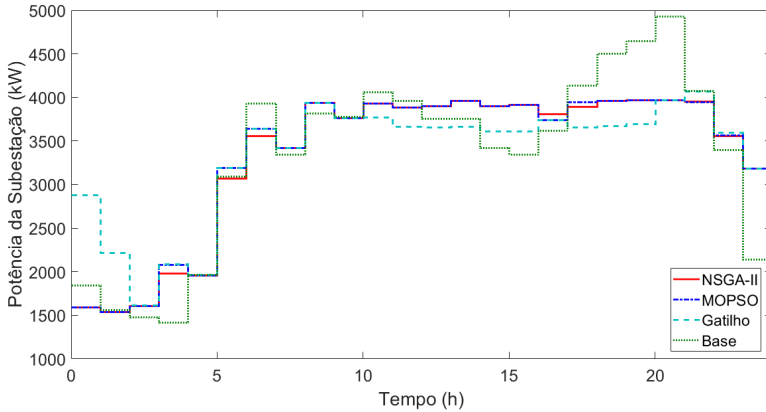


Fig. 16 Active power imported from the substation. Source: Author.

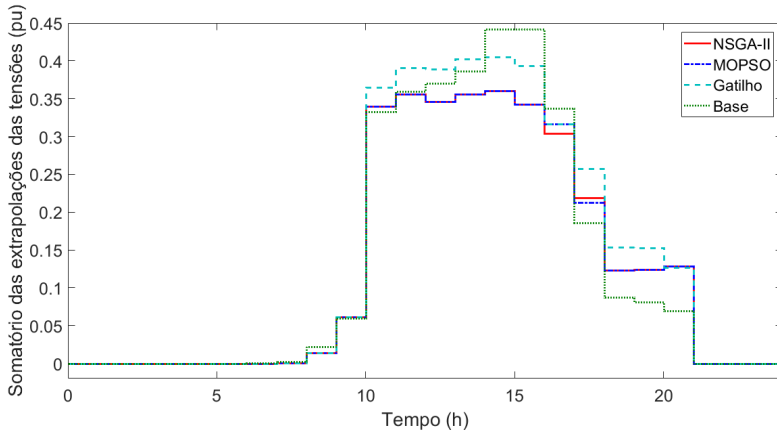


Fig. 17 Total voltage deviation. Source: Author.

Figure 18 shows the voltage at bus 60 (phase A), where the battery is installed. All three methods keep the voltage within regulatory limits throughout the day. Between 6 PM and 9 PM, the optimization algorithms better smooth voltage magnitudes than the trigger logic.

Figure 19 presents the phase A voltage profile at two buses: one at bus 3 and another at bus 79. While bus 3 shows little impact from storage, bus 79 displays clear improvements with heuristic strategies.

Figure 20 compares the number of tap changes on the voltage regulators. Metaheuristics offer better voltage control with reduced equipment wear. On the other hand, the trigger logic increases switching in some regulators.

Finally, Figure 21 presents the battery state of charge throughout the day. NSGA-II and MOPSO show similar behavior and keep the *SoC* at higher levels, promoting equipment longevity. The trigger logic shows greater fluctuation, reflecting its lower sensitivity to network dynamics.

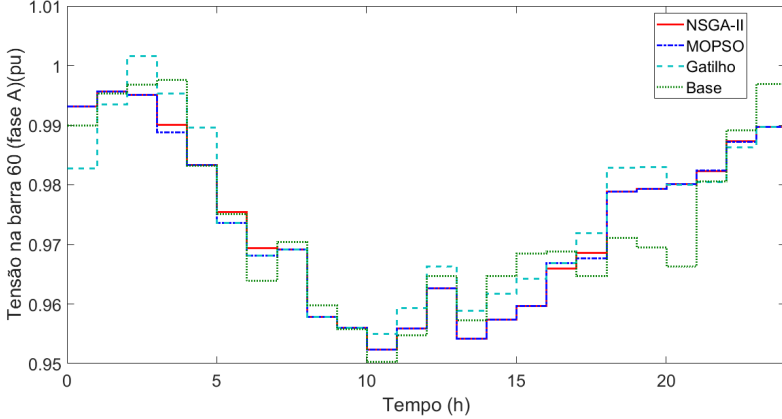


Fig. 18 Voltage at bus 60 (phase A). Source: Author.

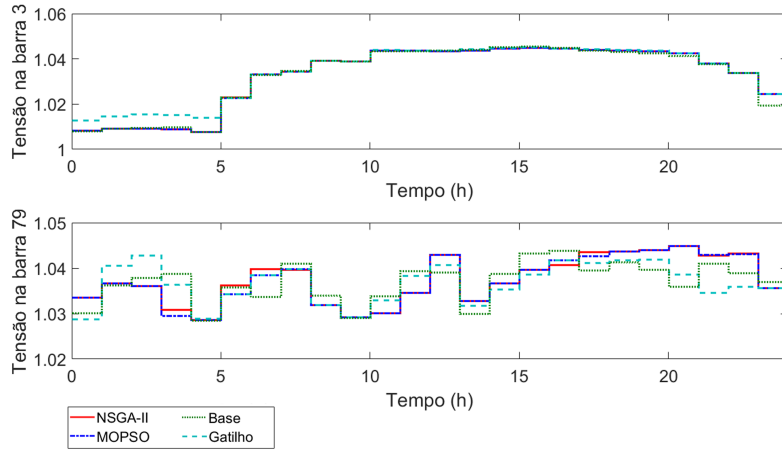


Fig. 19 Voltages at buses 3 and 79. Source: Author.

7.2.4 Additional Analyses

This section investigates the impact of the initial state of charge (SoC_0) of the battery on the results of the proposed energy management strategy, as well as the associated effects on active power losses. Table 9 presents the average and standard deviation of the quality metrics — hypervolume (H) and cardinality (C_R) — for 10 runs in three different SoC_0 scenarios: 25%, 50%, and 75%.

It is observed that changes in SoC_0 do not negatively affect the diversity or quality of the solutions. This is due to the fact that the simulation starts during the night, when demand is low, allowing the battery to be charged before the first demand peak. Therefore, the system remains flexible and efficient even under different initial conditions, which facilitates daily scheduling by the distribution network operator.

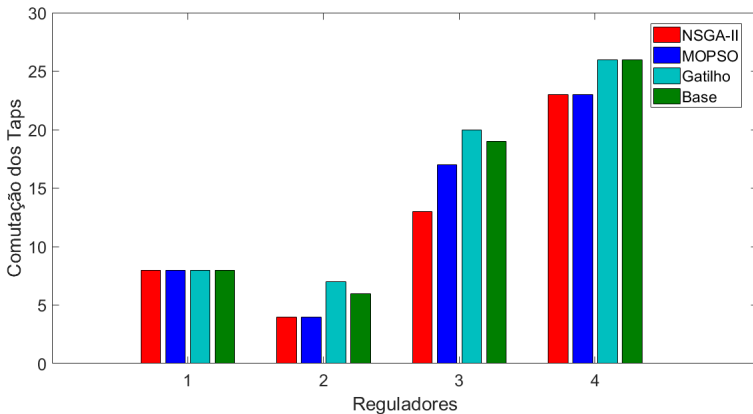


Fig. 20 Tap changes of voltage regulators. Source: Author.

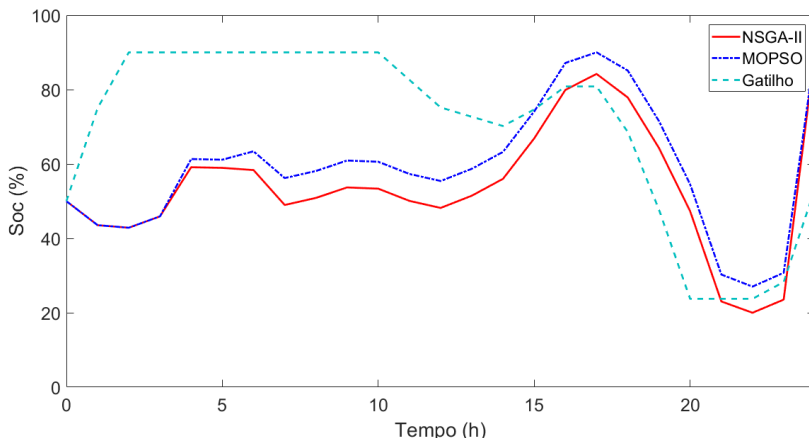


Fig. 21 Battery state of charge (SoC). Source: Author.

In addition to the influence of SoC_0 , the impact of management strategies on active energy losses was also analyzed. Table 10 presents the average and standard deviation of daily losses for the solutions obtained by the metaheuristics (NSGA-II and MOPSO), as well as for the trigger method and the base case without storage.

It is verified that all strategies involving energy storage resulted in lower active energy losses compared to the base case. However, unlike the results obtained for the 34-bus system, the trigger-based method performed better than the metaheuristic solutions. This suggests that if the operator's main objective is to minimize ohmic losses, it is advisable to explicitly include this criterion in the optimization problem formulation.

Table 9 Average and standard deviation of metrics for 10 runs with different initial SoC values in the IEEE 123-bus system. Source: Author.

Metric	Algorithm	SoC_0	Average	Std. Dev.
Hypervolume (H)	NSGA-II	25%	43.47	3.2
		50%	40.81	4.3
		75%	48.4	3.4
	MOPSO	25%	37.36	2.6
		50%	40.54	3.8
		75%	35.81	4.2
	NSGA-II	25%	199.0	1.7
		50%	199.3	1.1
		75%	199.0	1.7
Cardinality (C_R)	MOPSO	25%	60.2	5.5
		50%	103.1	6.4
		75%	77.0	1.9

Table 10 Active energy losses in the IEEE 123-bus system (in kWh). Source: Author.

	Base Case	Trigger	MOPSO		NSGA-II	
			Average	Std. Dev.	Average	Std. Dev.
Losses (kWh)	2506.12	2428.68	2498.66	37.40	2492.59	33.65

7.2.5 Computational Performance

Table 11 shows the average execution time (in minutes) for the metaheuristic step in MatLab and the power flow solution in OpenDSS for the IEEE 34 and 123-bus systems. The trigger method, which does not involve optimization, requires only a single execution in OpenDSS and completes in less than 10 seconds.

Table 11 Average computational time in minutes for each metaheuristic energy management method. Source: Author.

IEEE 34-Bus System		
Method	MatLab	OpenDSS
NSGA-II	30.2	80.4
MOPSO	32.4	87.6
IEEE 123-Bus System		
Method	MatLab	OpenDSS
NSGA-II	30.8	99.8
MOPSO	36.6	101.4

The results indicate that NSGA-II has a slight advantage in computational time, both in the optimization and simulation stages. In OpenDSS, the 123-bus system requires more time due to its greater structural complexity. It is worth noting, however, that these times may vary depending on the computational environment, programming languages, or use of parallel processing techniques.

8 Conclusion

This paper presented operational strategies for energy storage systems in distribution networks with photovoltaic generation, highlighting their benefits in the context of increasing penetration of renewable sources. Two IEEE test feeders were modeled in OpenDSS and coupled with *MatLab* for day-ahead planning, considering battery operation via two methods: a trigger-based logic using substation power and a multi-objective optimization approach using NSGA-II and MOPSO.

The proposed model aims to reduce load demand peaks, voltage deviations, and regulator tap operations, while respecting physical, operational, and battery lifetime constraints. Additionally, the influence of the initial state of charge, ohmic losses, and solution quality (hypervolume, cardinality, and computational time) were analyzed.

The results showed that the trigger-based approach has limited performance in scenarios with multiple or long-lasting peaks and may even worsen voltage deviations. On the other hand, the metaheuristic methods especially NSGA-II showed superior performance across all evaluated criteria, particularly in reducing tap changes without compromising voltage regulation. It was also observed that the storage system helps reduce power losses even without this being an explicit objective, and that different SoC_0 values had little impact when the simulation starts during low-demand periods.

As future work, it is suggested to investigate the effect of SoC_0 under high-load start conditions, to include losses as an explicit optimization objective, to evaluate new algorithms, apply additional quality metrics, and explore scenarios with multiple storage systems.

Acknowledgments

The authors thank FAPEMIG, CNPq, Capes, and INERGE for their support. The authors also thank CEPEL for granting permission to use the academic software versions of Anatem.

Declarations - Not applicable

Data availability

Data will be provided under request.

Appendix A

A.1 Load Curves

The numerical data of the load curves, presented in Table A1, are time series representing the electric energy demand throughout the day.

Table A1 Load Curve. Source: Adapted from [43].

Hour (h)	Residential Load Factor (pu)	Industrial Load Factor (pu)
1	0.59	0.15
2	0.48	0.19
3	0.44	0.22
4	0.41	0.25
5	0.55	0.41
6	0.85	0.65
7	1.01	1.01
8	0.80	1.25
9	0.89	1.55
10	0.91	1.65
11	1.07	1.73
12	1.12	1.55
13	1.18	1.21
14	1.05	1.62
15	0.93	1.65
16	0.92	1.57
17	1.02	1.35
18	1.16	1.15
19	1.31	0.65
20	1.39	0.55
21	1.55	0.35
22	1.30	0.25
23	1.09	0.21
24	0.69	0.15

A.2 Photovoltaic Units

The numerical data shown in Figure A1 and detailed in Tables A2, A3, and A4 are used to compute the power generated by the *PVsystem* element as a function of its daily irradiation, temperature, and inverter efficiency.

Table A2 Correction factor of panel power for different temperatures. Source: Adapted from [49].

Temperature (°C)	PMP Correction Factor (pu)
0	1.2
25	1.0
75	0.8
100	0.6

The photovoltaic units installed in the IEEE 123 and 34-bus systems are shown in Tables A5, A6, and A7.

Fig. A1 Characteristic curves of the *PVsystem* model in OpenDSS. Source: Adapted from [49].

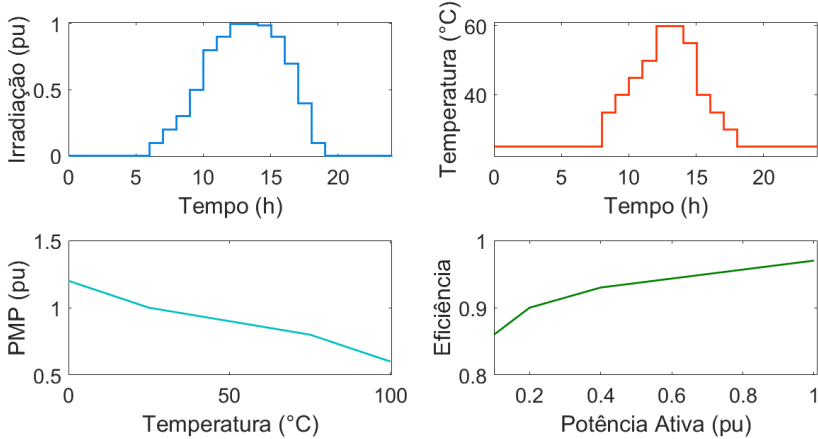


Table A3 Inverter efficiency curve. Source: Adapted from [49].

Irradiance (pu)	Efficiency (%)
0.1	86
0.2	90
0.4	93
1.0	97

Table A4 Irradiance and temperature curve of the *PVsystem* panel. Source: Adapted from [43].

Hour (h)	Irradiance (pu)	Temperature (°C)	Hour (h)	Irradiance (pu)	Temperature (°C)
1	0	25	13	1	60
2	0	25	14	1	60
3	0	25	15	0.99	55
4	0	25	16	0.9	40
5	0	25	17	0.7	35
6	0	25	18	0.4	30
7	0.1	25	19	0.1	25
8	0.2	25	20	0	25
9	0.3	35	21	0	25
10	0.5	40	22	0	25
11	0.8	45	23	0	25
12	0.9	50	24	0	25

Table A5 Photovoltaic units installed in the IEEE 123-bus system. Source: Author.

Bus	No. of Phases	Phases	Pmpp (kW)
3	1	C	6.2
5	1	C	30
7	3	A, B, C	12.4
8	3	A, B, C	15.5
9	1	A	6.2
12	1	B	30
13	3	A, B, C	6.2
14	1	A	8.25
15	1	C	8.25
16	3	A, B, C	100
21	3	A, B, C	100
22	1	B	10.3
24	1	C	30
25	3	A, B, C	8.25
26	2	A, C	6.2
28	3	A, B, C	100
29	3	A, B, C	12.4
30	3	A, B, C	30
31	1	C	10.3
32	1	C	6.2
33	1	A	10.3
36	2	A, B	100
38	1	B	12.4
41	1	C	8.25
42	3	A, B, C	1.8
45	1	A	10.3
46	1	A	8.25
48	3	A, B, C	1.8
49	3	A, B, C	15.5
37	1	A	10.3
50	3	A, B, C	60

Table A6 Photovoltaic units installed in the IEEE 123-bus system (continued). Source: Author.

Bus	No. of Phases	Phases	Pmpp (kW)
51	3	A, B, C	60
55	3	A, B, C	15.5
56	3	A, B, C	8.25
57	3	A, B, C	100
58	1	B	12.4
59	1	B	1.8
65	3	A, B, C	12.4
68	1	A	1.8
69	1	A	12.4
70	1	A	6.2
71	1	A	10.3
72	3	A, B, C	1.8
73	1	C	6.2
74	1	C	60
75	1	C	12.4
76	3	A, B, C	15.5
77	3	A, B, C	8.25
78	3	A, B, C	10.3
79	3	A, B, C	12.4
81	3	A, B, C	6.2
82	3	A, B, C	30
84	1	C	15.5
85	1	C	30
86	3	A, B, C	8.25
88	1	A	12.4
90	1	B	60
91	3	A, B, C	15.5
92	1	C	60
95	3	A, B, C	1.8
96	1	B	10.3
98	3	A, B, C	1.8
99	3	A, B, C	10.3
100	3	A, B, C	15.5
101	3	A, B, C	100
103	1	C	30
106	1	B	60
107	1	B	15.5
109	1	A	8.25
111	1	A	6.2
110	1	A	10.3
112	1	A	6.2
113	1	A	12.4
135	3	A, B, C	1.8
152	3	A, B, C	6.2
160	3	A, B, C	30
197	3	A, B, C	1.8
450	3	A, B, C	100

Table A7 Photovoltaic units installed in the IEEE 34-bus system. Source: Author.

Bus	No. of Phases	Phases	Pmpp (kW)
802	3	A, B, C	6.2
806	3	A, B, C	6.2
808	3	A, B, C	8.25
810	1	B	10.3
812	3	A, B, C	12.4
814	3	A, B, C	6.2
850	3	A, B, C	10.3
816	3	A, B, C	30
818	1	A	1.8
820	1	A	30
822	1	A	15.5
824	3	A, B, C	1.8
826	1	B	10.3
828	3	A, B, C	60
830	3	A, B, C	30
854	3	A, B, C	60
856	1	B	10.3
852	3	A, B, C	60
832	3	A, B, C	1.8
888	3	A, B, C	30
890	3	A, B, C	40
858	3	A, B, C	60
864	1	A	60
834	3	A, B, C	16.5
842	3	A, B, C	60
844	3	A, B, C	12.9
846	3	A, B, C	30
848	3	A, B, C	60
860	3	A, B, C	10.3
836	3	A, B, C	16.5
840	3	A, B, C	15.5
862	3	A, B, C	30
838	1	B	60

References

- [1] Lima, M.A., Mendes, L.F.R., Mothé, G.A., Linhares, F.G., de Castro, M.P.P., da Silva, M.G., Sthel, M.S.: Renewable energy in reducing greenhouse gas emissions: Reaching the goals of the paris agreement in brazil. Environmental Development **33**, 100504 (2020). <https://doi.org/10.1016/j.envdev.2020.100504>
- [2] ANEEL: Geração Distribuída. Disponível em: <https://www.gov.br/aneel/pt-br/assuntos/geracao-distribuida>. Acesso em: 13-Setembro-2022
- [3] da Silva, A.V., Rato, T.A.T.: Navigating the transition: The impacts of electricity tariff regulation on distributed generation in brazil. Utilities Policy **90**, 101794 (2024). <https://doi.org/10.1016/j.jup.2024.101794>. Acesso em: 15 de jul. de 2025
- [4] da Silva, A.V., Rato, T.A.T.: Navigating the transition: The impacts of electricity tariff regulation on distributed generation in brazil. Utilities Policy **90**, 101794 (2024). <https://doi.org/10.1016/j.jup.2024.101794>
- [5] Nguyen, C., Power, A.F.-I., Society, E., undefined 2008: Impacts of merit order based dispatch on transfer capability and static voltage stability. ieeexplore.ieee.org
- [6] Miranda, R.F.C.: O papel da transmissão de eletricidade inter e intraregional em modelos de expansão e operação do sistema energético com forte penetração de fontes renováveis. PhD thesis, Tese de Doutorado, COPPE/UFRJ, Rio de Janeiro, Brazil (2018)
- [7] Smith, J., Li, X., Kumar, A.: Role of battery energy storage systems: A comprehensive review on control methodologies, ems frameworks, and their impact on grid stability and power quality. Journal of Energy Storage **50**, 102345 (2025). <https://doi.org/10.1016/j.est.2024.102345>
- [8] Sistemas de Armazenamento em Baterias - Aplicações e Questões Relevantes para o Planejamento. Disponível em: "https://www.epe.gov.br/sites-pt/publicacoes-dados-abertos/publicacoes/PublicacoesArquivos/publicacao-441/EPE-DEE-NT-098_2019_Baterias%20no%20planejamento.pdf". Acesso em: 27-Julho-2022
- [9] PRODIST: Regras e Procedimentos de Distribuição (Prodist). Disponível em: <https://www.gov.br/aneel/pt-br/centrais-de-conteudos/procedimentos-regulatorios/prodist>. Acesso em: 23-Dezembro-2024
- [10] Projetos de Chamada Estratégica. Disponível em: <https://www.gov.br/aneel/pt-br/assuntos/pesquisa-e-desenvolvimento/projetos-de-chamada-estrategica>. Acesso em: 03-Junho-2024

- [11] Leal, R.S., Hartmann, L.V., Gehrke, C.S., Salvadori, F.: Análise de tecnologias para sistemas de armazenamento de energia. In: Congresso Brasileiro de Automática-CBA, vol. 2 (2020)
- [12] Koohi-Fayegh, S., Rosen, M.A.: A review of energy storage types, applications and recent developments. *Journal of Energy Storage* **27**, 101047 (2020). <https://doi.org/10.1016/j.est.2019.101047>
- [13] Maeyaert, L., Vandeveldt, L., Döring, T.: Battery storage for ancillary services in smart distribution grids. *Journal of Energy Storage* **30**, 101524 (2020)
- [14] Nagarajan, A., Ayyanar, R.: Design and strategy for the deployment of energy storage systems in a distribution feeder with penetration of renewable resources. *IEEE Transactions on Sustainable Energy* **6**(3), 1085–1092 (2014)
- [15] Wang, Y., Wang, B., Chu, C.-C., Pota, H., Gad, R.: Energy management for a commercial building microgrid with stationary and mobile battery storage. *Energy and Buildings* **116**, 141–150 (2016)
- [16] Shi, Y., Xu, B., Wang, D., Zhang, B.: Using battery storage for peak shaving and frequency regulation: Joint optimization for superlinear gains. *IEEE Transactions on Power Systems* **33**(3), 2882–2894 (2017)
- [17] Zeraati, M., Golshan, M.E.H., Guerrero, J.M.: Distributed control of battery energy storage systems for voltage regulation in distribution networks with high pv penetration. *IEEE Transactions on Smart Grid* **9**(4), 3582–3593 (2016)
- [18] Lokeshgupta, B., Sivasubramani, S.: Multi-objective home energy management with battery energy storage systems. *Sustainable Cities and Society* **47**, 101458 (2019). <https://doi.org/10.1016/j.scs.2019.101458>
- [19] Engels, J., Claessens, B., Deconinck, G.: Optimal combination of frequency control and peak shaving with battery storage systems. *IEEE Transactions on Smart Grid* **11**(4), 3270–3279 (2020). <https://doi.org/10.1109/TSG.2019.2963098>
- [20] Optimization of fuzzy energy-management system for grid-connected microgrid using nsga-ii. *ieeexplore.ieee.org*, 51 (2021). <https://doi.org/10.1109/tcyb.2020.3031109>
- [21] Zamzam, A.S., Dall’Anese, E., Sidiropoulos, N.D.: Optimal distributed energy storage management using relaxed dantzig-wolfe decomposition. In: 2018 IEEE Conference on Decision and Control (CDC), pp. 2396–2401 (2018). IEEE

- [22] Krata, J., Saha, T.K.: Real-time coordinated voltage support with battery energy storage in a distribution grid equipped with medium-scale pv generation. *IEEE Transactions on Smart Grid* **10**(3), 3486–3497 (2019). <https://doi.org/10.1109/TSG.2018.2828991>
- [23] Bazrafshan, M., Gatsis, N., Zhu, H.: Optimal power flow with step-voltage regulators in multi-phase distribution networks. *IEEE Transactions on power systems* **34**(6), 4228–4239 (2019)
- [24] Joshi, K.A., Pindoriya, N.M., Srivastava, A.K.: A two-stage fuzzy multi-objective optimization for phase-sensitive day-ahead dispatch of battery energy storage system. *IEEE Systems Journal* **12**(4), 3649–3660 (2018)
- [25] Abdelkader, A., Rabeh, A., Mohamed Ali, D., Mohamed, J.: Multi-objective genetic algorithm based sizing optimization of a stand-alone wind/pv power supply system with enhanced battery/supercapacitor hybrid energy storage. *Energy* **163**, 351–363 (2018). <https://doi.org/10.1016/j.energy.2018.08.135>
- [26] Wang, S., Wang, K., Teng, F., Strbac, G., Wu, L.: An affine arithmetic-based multi-objective optimization method for energy storage systems operating in active distribution networks with uncertainties. *Applied Energy* **223**, 215–228 (2018). <https://doi.org/10.1016/j.apenergy.2018.04.037>
- [27] de Souza Silva, R.D.: Utilização de sistemas de armazenamento de energia em baterias no setor elétrico e as perspectivas para o Brasil (2021). <https://doi.org/10.38116/radar68art2>
- [28] Guo, Y., Zhao, C.: Islanding-aware robust energy management for microgrids. *IEEE Transactions on Smart Grid* **9**(2), 1301–1309 (2018). <https://doi.org/10.1109/TSG.2016.2585092>
- [29] Geramifar, H., Shahabi, M., Barforoshi, T.: Coordination of energy storage systems and dr resources for optimal scheduling of microgrids under uncertainties. *IET Renewable Power Generation* **11**(2), 378–388 (2017)
- [30] Yang, Z., Ghadamyari, M., Khorramdel, H., Seyed Alizadeh, S.M., Pirouzi, S., Milani, M., Banihashemi, F., Ghadimi, N.: Robust multi-objective optimal design of islanded hybrid system with renewable and diesel sources/stationary and mobile energy storage systems. *Renewable and Sustainable Energy Reviews* **148**, 111295 (2021). <https://doi.org/10.1016/j.rser.2021.111295>
- [31] Khaki, B., Das, P.: Sizing and placement of battery energy storage systems and wind turbines by minimizing costs and system losses. *arXiv preprint arXiv:1903.12029* (2019)

- [32] Karanki, S.B., Xu, D.: Optimal capacity and placement of battery energy storage systems for integrating renewable energy sources in distribution system. In: 2016 National Power Systems Conference (NPSC), pp. 1–6 (2016). <https://doi.org/10.1109/NPSC.2016.7858983>
- [33] Trivić, B., Savić, A.: Optimal allocation and sizing of bess in a distribution network with high pv production using nsga-ii and lp optimization methods. *Energies* **18**(5) (2025)
- [34] Liu, Y., Wu, X., Du, J., Song, Z., Wu, G.: Optimal sizing of a wind-energy storage system considering battery life. *Renewable Energy* **147**, 2470–2483 (2020)
- [35] Cao, M., Xu, Q., Qin, X., Cai, J.: Battery energy storage sizing based on a model predictive control strategy with operational constraints to smooth the wind power. *International Journal of Electrical Power & Energy Systems* **115**, 105471 (2020)
- [36] Yang, X.S.: Nature-Inspired Optimization Algorithms, (2020). <https://doi.org/10.1016/B978-0-12-821986-7.00002-0>
- [37] Deb, K., Pratap, A., Agarwal, S., Meyarivan, T.: A fast and elitist multi-objective genetic algorithm: Nsga-ii. *IEEE Transactions on Evolutionary Computation* **6**(2), 182–197 (2002). <https://doi.org/10.1109/4235.996017>
- [38] Kennedy, J., Eberhart, R.: Particle swarm optimization. In: Proceedings of ICNN'95-international Conference on Neural Networks, vol. 4, pp. 1942–1948 (1995). IEEE
- [39] Sierra, M.R., Coello, C.A.: Improving pso-based multi-objective optimization using crowding, mutation and-dominance. In: International Conference on Evolutionary Multi-criterion Optimization, pp. 505–519 (2005). Springer
- [40] Zitzler, E., Thiele, L.: Multiobjective evolutionary algorithms: a comparative case study and the strength pareto approach. *IEEE transactions on Evolutionary Computation* **3**(4), 257–271 (1999)
- [41] Dugan, R.C., McDermott, T.E.: An open source platform for collaborating on smart grid research. In: 2011 IEEE Power and Energy Society General Meeting, pp. 1–7 (2011). <https://doi.org/10.1109/PES.2011.6039829>
- [42] Bansal, A.K., Gupta, R., Kumar, R.: Optimization of hybrid pv/wind energy system using meta particle swarm optimization (mpso). In: India International Conference on Power Electronics 2010 (IICPE2010), pp. 1–7 (2011). IEEE

- [43] Coelho, F.C.R., Peres, W., Silva, I.C., Dias, B.H.: Empirical continuous metaheuristic for multiple distributed generation scheduling considering energy loss minimisation, voltage and unbalance regulatory limits. *IET Generation, Transmission and Distribution* **14**, 3301–3309 (2020). <https://doi.org/10.1049/IET-GTD.2019.1860>
- [44] Gan, L.K., Shek, J.K.H., Mueller, M.A.: Hybrid wind–photovoltaic–diesel–battery system sizing tool development using empirical approach, life-cycle cost and performance analysis: A case study in scotland. *Energy Conversion and Management* **106**, 479–494 (2015). <https://doi.org/10.1016/j.enconman.2015.09.029>
- [45] Santos, A., Oliveira, L., Dias, B., Oliveira, J.: Otimização da operação de baterias em sistemas de distribuição de energia elétrica. In: XII Latin-American Congress on Electricity Generation and transmission-CLAGTEE (2017)
- [46] IEEE PES: Distribution Test Feeders. Disponível em: <https://site.ieee.org/pes-testfeeders/>. Acesso em: 25-Maio-2022 (2021)
- [47] Resources – IEEE PES Test Feeder. Disponível em: <https://cmte.ieee.org/pes-testfeeders/resources/>. Acesso em: 18-Junho-2022
- [48] Alegria, E., Brown, T., Minear, E., Lasseter, R.H.: Certs microgrid demonstration with large-scale energy storage and renewable generation. *IEEE Transactions on Smart Grid* **5**(2), 937–943 (2014). <https://doi.org/10.1109/TSG.2013.2286575>
- [49] Ricardo, P., Freitas, R.D.: Impacto de funções inteligentes de inversores de sistemas fotovoltaicos na operação de redes de distribuição de energia elétrica. (2020). <https://doi.org/10.11606/D.3.2019.TDE-20032020-074934>